Intraretinal Correlates of Reticular Pseudodrusen Revealed by Autofluorescence and En Face OCT

Maarjaliis Paavo,[1] Winston Lee,[1] John Merriam,[1] Srilaxmi Bearelly,[1] Stephen Tsang,[1,2] Stanley Chang,[1] and Janet R. Sparrow[1,2]

[1]Department of Ophthalmology, Columbia University Medical Center, New York, New York, United States
[2]Department of Pathology and Cell Biology, Columbia University Medical Center, New York, New York, United States

Correspondence: Janet R. Sparrow, Department of Ophthalmology, Columbia University Medical Center, 635 W. 165th Street, New York, NY 10032, USA; jrs88@cumc.columbia.edu.

Submitted: June 1, 2017
Accepted: August 8, 2017

Citation: Paavo M, Lee W, Merriam J, et al. Intraretinal correlates of reticular pseudodrusen revealed by autofluorescence and en face OCT. *Invest Ophthalmol Vis Sci*. 2017;58:4769–4777. DOI:10.1167/iovs.17-22338

Purpose. We sought to determine whether information revealed from the reflectance, autofluorescence, and absorption properties of RPE cells situated posterior to reticular pseudodrusen (RPD) could provide insight into the origins and structure of RPD.

Methods. RPD were studied qualitatively by near-infrared fundus autofluorescence (NIR-AF), short-wavelength fundus autofluorescence (SW-AF), and infrared reflectance (IR-R) images, and the presentation was compared to horizontal and en face spectral domain optical coherence tomographic (SD-OCT) images. Images were acquired from 23 patients (39 eyes) diagnosed with RPD (mean age 80.7 ± 7.1 [SD]; 16 female; 4 Hispanics, 19 non-Hispanic whites).

Results. In SW-AF, NIR-AF, and IR-R images, fundus RPD were recognized as interlacing networks of small scale variations in IR-R and fluorescence (SW-AF, NIR-AF) intensities. Darkened foci of RPD colocalized in SW-AF and NIR-AF images, and in SD-OCT images corresponded to disturbances of the interdigitation (IZ) and ellipsoid (EZ) zones and to more pronounced hyperreflective lesions traversing photoreceptor-attributable bands in SD-OCT images. Qualitative assessment of the outer nuclear layer (ONL) revealed thinning as RPD extended radially from the outer to inner retina. In en face OCT, hyperreflective areas in the EZ band correlated topographically with hyporeflective foci at the level of the RPE.

Conclusions. The hyperreflective lesions corresponding to RPD in SD-OCT scans are likely indicative of degenerating photoreceptor cells. The darkened foci at positions of RPD in NIR-AF and en face OCT images indicate changes in the RPE monolayer with the reduced NIR-AF and en face OCT signal suggesting a reduction in melanin that could be accounted for by RPE thinning.

Keywords: age-related macular degeneration, AMD, bisretinoid, fundus autofluorescence, lipofuscin, reticular pseudodrusen, spectral-domain optical coherence tomography, scanning laser ophthalmoscope

Fundus features that are indicative of vision-threatening age-related macular degeneration (AMD) include soft drusen and pigmentary abnormalities. In high resolution images of intermediate and advanced AMD, reticular pseudodrusen (RPD,[1] also referred to as subretinal drusenoid deposits [SDD][2]) constitute an additional lesion that also is observed frequently. While not readily detectable in color fundus images, RPD, when present, are prominently displayed in near-infrared reflectance (IR-R) and short wavelength autofluorescent (SW-AF) fundus images and by confocal scanning laser ophthalmoscopy (cSLO).[3–6] In fundus images RPD manifest as interlacing networks of small scale variations in IR-R and SW-AF intensities.[4–6] RPD patterns consist of interconnected bands of hypoautofluorescence or hyporeflectance that assume a reticular pattern (ribbon-like subtype); alternatively, the darkened lesions can present as confluent rounded or oval forms, some of which have a bright central dot and, thus, form target-like configurations.[2,7–10]

RPD are reported to be most obvious in the superior perifovea, the area of retina having the greatest density of rods[11] and highest levels of RPE lipofuscin.[12,13] The presence of RPD is associated strongly with impaired dark adaptation[14] and reduced scotopic sensitivity measured by microperimetry[15] and with delays in implicit times of multifocal electroretinography (mfERG).[16] RPD almost always are present bilaterally.[2,3,17,18] The presence of RPD in the fundus coincides with features of AMD, such as large sub-RPE drusen and pigmentary changes, and the association is highest with geographic atrophy (GA).[19] Indeed, the progression of GA was more frequent in fundus areas exhibiting RPD compared to those areas free of RPD.[20] Moreover, AMD and RPD share susceptibility factors that include increasing age, smoking, and known risk genotypes.[19]

The morphologic correlates of RPD have been debated. Some investigators have attributed RPD to disease-related structural variants within the choroidal vasculature.[9,21,22] Other investigators have demonstrated, using spectral domain–optical coherence tomography (SD-OCT) images, that these lesions are located in the outer retina. In SD-OCT scans, RPD are described typically as accumulations within the subretinal space.[2,23] They have been attributed to unphagocytosed outer segments or debris buildup from RPE[8,24,25] and the cause of degeneration of overlying

Table. Summary of Demographic and Clinical Findings

				BCVA logMAR		*BIMR Classification	
Patient	Age	Sex	Race/Ethnicity	OD	OS	OD	OS
1	55.4	F	Hispanic	0.00	0.00	0	0
2	83.8	M	White	0.88	0.54	4	4
3	76.8	F	White	0.10	0.00	3	3
4	79.2	F	White	0.00	0.18	3	3
5	83.9	F	White	0.20	1.30	3	4
6	78.6	F	White	0.30	0.10	3	3
7	88.6	M	White	0.70	0.10	4	3
8	84.6	F	Hispanic	0.39	0.39	4	4
9	81.7	F	White	0.10	0.20	0	0
10	74.9	F	White	0.10	0.20	3	3
11	79.6	F	Hispanic	0.39	0.10	3	2
12	79.9	F	White	1.30	0.10	4	4
13	80.3	F	White	0.10	0.88	4	4
14	85.8	F	White	0.39	0.88	3	2
15	80.6	F	White	0.10	0.39	3	3
16	86.9	M	White	0.00	0.18	2	4
17	72.4	F	Hispanic	0.00	0.00	4	4
18	89.1	M	White	0.54	0.10	4	3
19	80.2	F	White	0.10	0.47	3	3
20	84.5	M	White	0.00	0.00	3	3
21	80.4	F	White	0.87	0.30	4	3
22	80	M	White	1.3	0.1	2	2
23	89.7	M	White	0.2	0.2	0	0

* Grading according to clinical classification of Beckman Initiative for Macular Research.

photoreceptor cells.[26] In SD-OCT scans, RPD correspond to well-defined conical or triangular hyperreflective deposits on the apical side (toward the cornea) of the RPE monolayer,[24] as opposed to conventional drusen that form on the basal/scleral side of the RPE. The material itself, for the most part, has a molecular composition different than sub-RPE drusen.[8,27]

Precise phenotyping is essential to the appropriate selection of patients for clinical studies aimed at evaluating treatment efficacy. Several studies have emphasized the importance of defining RPD using multimodal imaging that includes cSLO and SD-OCT modalities.[15,18,28] We also applied the modalities of near-infrared fundus autofluorescence (NIR-AF) and en face SD-OCT to the study of RPD. NIR-AF is a fundus imaging modality with a signal that derives primarily from RPE melanin[29] and that, to our knowledge, has not been applied previously to probe the intraretinal correlates of RPD. We determined whether information revealed from the reflectance, autofluorescence, and absorption properties of RPE cells situated posterior to an RPD lesion could provide insight into the origins and structure of RPD.

Methods

Patients

We studied 23 patients recruited prospectively at Columbia University with a clinical diagnosis of RPD. Patient ages ranged from 55.4 to 89.7 years. The patients underwent a complete ophthalmic examination including evaluation of best-corrected visual acuity. Clinical and demographic data are presented in the Table. AMD was classified according to the 5-stage image-based criteria established by the Beckman Initiative for Macular Research[30] (Table). Patients were included in the study if reticular pseudodrusen were determined to be present in an eye when detected by IR-R, NIR-AF, SW-AF, and SD-OCT images.

All procedures adhered to the tenets of the Declaration of Helsinki and written informed consent was obtained from all patients after full explanation of the procedures. The study was performed with the approval of the institutional review board of Columbia University, and all patients were enrolled in accordance with the tenets set out in the Declaration of Helsinki. Informed consent was obtained before enrollment.

SW-AF Imaging

SW-AF images (30° × 30° field, 488 nm excitation) were acquired using a scanning laser ophthalmoscope (cSLO; Spectralis HRA+OCT; Heidelberg Engineering, Heidelberg, Germany) in the high-resolution mode (8.9 frames/sec; 9–12 frames/sec; up to 100 frames, automatic real-time tracking). Pupils were dilated to at least 7 mm with topical 1% tropicamide and 2.5% phenylephrine. The fundus was exposed for 20 to 30 seconds to bleach rhodopsin during focus and alignment; detector sensitivity was adjusted to prevent gray level (GL) saturation (<175) and frames were aligned and saved in nonnormalized mode.

NIR-AF Imaging

NIR-AF images (30° × 30° field, 787 nm excitation, >830 nm emission) were acquired with the HRA2-SLO (Heidelberg Engineering) using the indocyanine-green angiography mode (787 nm excitation) and a sensitivity of 96. To obtain high-quality images the eye-tracking function was used, and 100 single frames were averaged and saved in normalized mode. Images were registered using i2kRetina software (DualAlign LLC, Clifton Park, NY USA).

SD-OCT Imaging

SD-OCT images were acquired with the Spectralis (Heidelberg Engineering) as horizontal 9 × 9 mm scans (870 nm; 7 microM

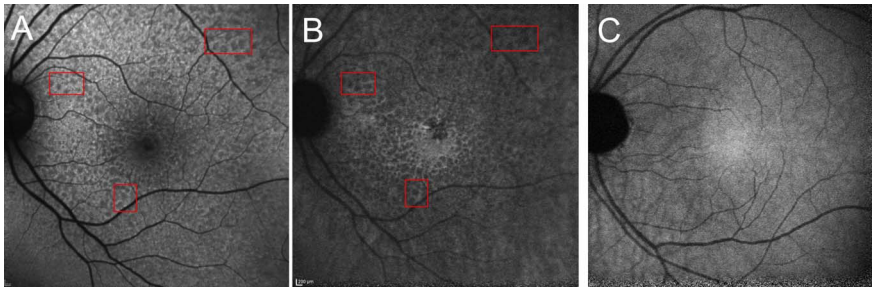

FIGURE 1. Representative fundus images of P9 exhibiting reticular pseudodrusen (**A, B**). Images of reticular pseudodrusen were acquired as SW-AF (**A**) and NIR-AF (**B**). Examples of corresponding areas in (**A**) and (**B**) are shown in *red rectangles* for comparison. NIR-AF in a healthy eye (**C**).

axial resolution) through the macula acquired in high-resolution mode with averaging of 100 single scans. The scans were registered automatically to a simultaneously acquired IR-R (820 nm) fundus image, which was later used for point-to-point correlation with other fundus images. Nomenclature used to identify reflectivity bands in SD-OCT images were as published.[31] Increased signal transmission posterior to RPD in SD-OCT scans was defined as an RPD-associated column of hyperreflectivity projecting into the choroid. The width of this increased transmission corresponded approximately to the width of the RPD as viewed along the RPE/Bruch's reflectivity layer.

Images also were acquired on a high definition OCT (HD-OCT Cirrus Model 5000; Carl Zeiss Meditec, Dublin, CA) as angiography (6×6 or 3×3 mm scanning area) or macular cube volume scans (6×6 mm; 512×128 scans; 5 microM axial resolution; 840 nm). The scans were captured together with a near infrared fundus image (750 nm). Using HD-OCT software (version 9.5.0.8211; Carl Zeiss Meditec) en face maps (C-scans) were generated at the level of the ellipsoid zone (offset −45, thickness 21 μm) and RPE-Bruch's membrane (offset 0, thickness 21 μm).

Outer Retinal Reflectivity Analysis

OCT layer reflectivity, or local pixel gray level values, were analyzed on single horizontal and volumetric B scans from the Spectralis HRA+ OCT using the open-source analysis software Fiji.[32] Reflectivity profiles along the entire width of the B scan were generated by segmenting the full length of the RPE layer while cross-layer profiles were generated from straight lines positioned perpendicularly with respect to the RPE band.

RESULTS

SW-AF, NIR-AF, IR-R, and SD-OCT images were analyzed in 39 eyes of 23 patients aged 55.4 to 89.7 years (mean age, 80.7 ± 7.1 SD years; Table); the advanced age of the cohort was consistent with previous studies reporting that cohorts of RPD patients tend to be older than non-RPD AMD groups.[4,7,20,33,34] There were 16 women and 4 patients self-identified as Hispanic, while the rest were white. RPD were identified in all patients (39 eyes). Classical sub-RPE drusen were present in 33/39 eyes and 15 eyes presented with late AMD (neovascular and/or GA; category 4; Beckman Initiative for Macular Research[30]).

As previously reported, RPD patterning in SW-AF images (39/39 eyes) took the form of repeating units of hypoautofluorescence visualized as interlacing ribbons or circular to oval darkened foci surrounded by brighter annuli (Figs. 1A, 2A). Matching gray scale variations were observed in the NIR-AF images; signals in the latter images were derived largely from RPE melanin. The darkened foci of the RPD lesion and the brighter annuli colocalized in SW-AF and NIR-AF images (Figs. 1B, 2B). Because of what appeared to be better contrast, RPD could be visualized more readily in the NIR-AF images. As shown in Figure 1, the NIR-AF signal in the central fundus of healthy eyes is considerably elevated as has been described previously[29] (Fig. 1C). The fundus patterning associated with RPD generally extended into this area of high NIR-AF emission, noticeably altering its contours (Figs. 1B, 2B). In some eyes (for instance P4; 13/39 eyes) exhibiting RPD, the NIR-AF signal emanating from the fovea and perifovea was reduced (Figs. 1B, 2B). In contrast to the brighter NIR-AF pattern in healthy eyes, the normal SW-AF signal in the central macula is reduced due to the presence of macular pigment extending to an eccentricity of 6° to 8° from the fovea (maximum absorbance, 460 nm).[35] In SW-AF images, few RPD were visible inside the spatial limits of this area and the RPD did not alter the distribution of macular pigment (Figs. 1A, 2A). Thus, NIR-AF imaging was advantageous for the detection of RPD in foveal and perifoveal retina.

Reticular pseudodrusen also were identified as hyporeflectant aberrations in IR-R images (Fig. 2C), as described previously.[2–6,10] In IR-R images, RPD could be more discernible centrally perhaps at least in part due to the higher melanin optical density.[36]

In SD-OCT images, the hypo-AF foci identified as RPD in NIR-AF images corresponded to hyperreflective changes. In some cases, these changes were characterized by a diffuse hyperreflectivity of the interdigitation zone (IZ) and subtle undulations that altered the contour of the ellipsoid zone (EZ) band (39/39 eyes; Figs. 2E, 3C),[2,10,37–39] consistent with Stage 2 of a previously described grading scheme.[2] These aberrations corresponded to darkened foci in SW-AF and NIR-AF images. In other cases (34/39 eyes), RPD observed in NIR-AF and SW-AF fundus images corresponded to hyperreflective foci in SD-OCT images that traversed photoreceptor-attributable bands and extended through the EZ (Stage 3 in the report of Zweifel et al.[2]; Figs. 2E, 3A, 3B). As hyperreflective deposits, these aberrations tended to interrupt the EZ and external limiting membrane (ELM) rather than displace these bands and the EZ and ELM were continuous on either side of the RPD (34/39 eyes; Figs. 2E, 3). Radial extension of the hyperreflective deposits as far as the outer nuclear layer (ONL)–attributable band was readily visible due to the contrast with the hyporeflectivity of the latter (Fig. 2E). ONL thinning, judged qualitatively, was observed (34/39 eyes) when the hyperreflective lesion extended through IZ- and EZ-attributable bands. In the case of some RPD (10 eyes), increased transmission of signal was observed on the choroidal side of the RPD (Figs. 3A, 3B). Bright spots were visible within some darkened foci of SW-AF, NIR-AF, and IR-R images when the peak of the pyramidal- or barrel-shaped deposit projected through

Investigative Ophthalmology & Visual Science

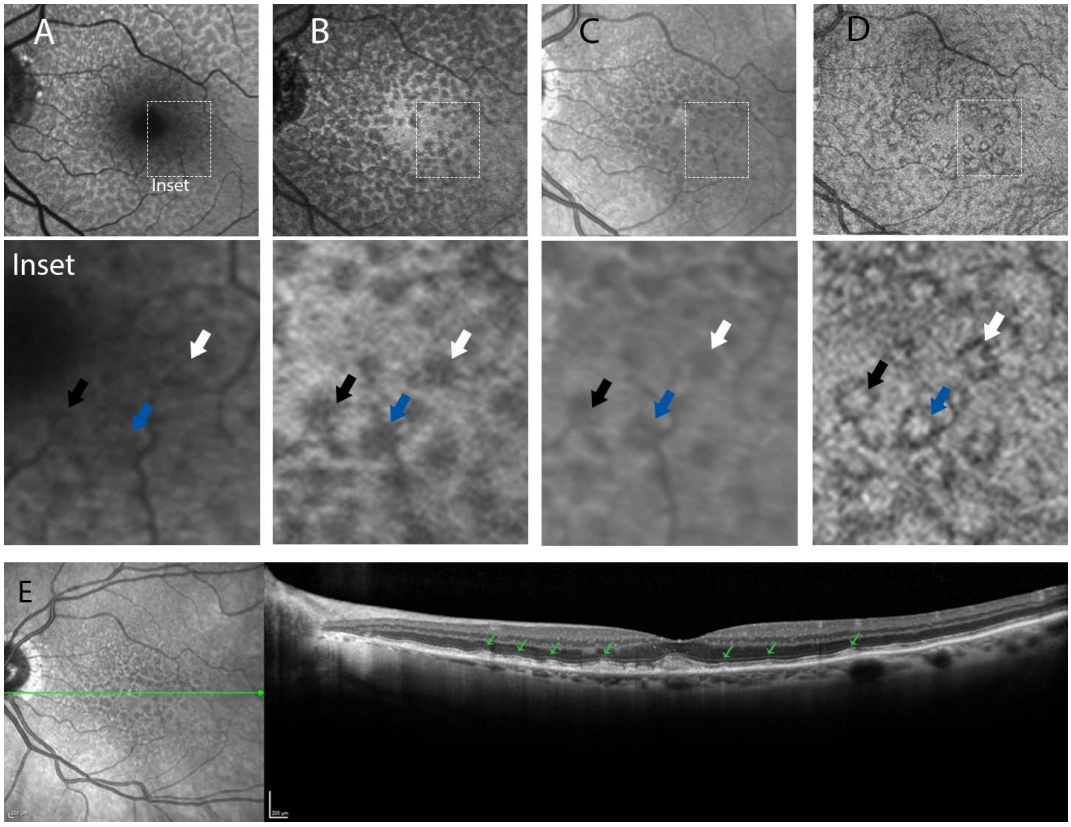

Figure 2. Multimodal imaging of reticular pseudodrusen in P4. RPD colocalize as darkened foci in SW-AF (**A**), NIR-AF (**B**), and IR-R (**C**) images acquired with Spectralis (SW-AF, IR-R) and HRA2 (Heidelberg Engineering). In en face SD-OCT images acquired with Zeiss Cirrus (coronal) at the level of EZ. (**D**) RPD present as multiple reflective circles exhibiting borders of reduced reflectivity (*dark*). Examples of corresponding lesions are indicated by *black*, *blue*, and *white arrows*. *Magnified insets* are shown for (**A**–**D**). The foveal hyperreflective spot in the IR-R image (**C**) is a normal "umbo."[36] (**E**) Reticular pseudodrusen as revealed in a horizontal SD-OCT image. *Horizontal axis* of the SD-OCT scan in (**E**) is indicated by *green line* in the IR-R image. RPD can present as intermittent thickening of the IZ and EZ bands (*green arrows*).

the EZ (16/39 eyes). These are the target lesions described previously in IR-R images.[7,15,39,40]

En face (coronal) OCT imaging (32/39 eyes) at the selected depth of the EZ revealed multiple small round hyperreflective abnormalities (Fig 2D) that colocalized with RPD lesions observed in SW-AF, NIR-AF, and IR-R images. B-scan and en face structural images were acquired with the Zeiss HD-OCT Model 5000 instrument from 19 patients (32/39 eyes) with RPD (Fig. 4). The hyperreflective foci at the EZ level corresponded to foci of diminished reflectivity in images positioned at the RPE (Fig. 4).

We measured reflectivity intensities within the RPE/Bruch's attributable SD-OCT layer in 18 patients (18 eyes) exhibiting RPD disease; patients with macular atrophy and/or choroidal neovascular disease were excluded. Scans exhibiting excessive signal noise or nonuniformity of reflectance throughout the

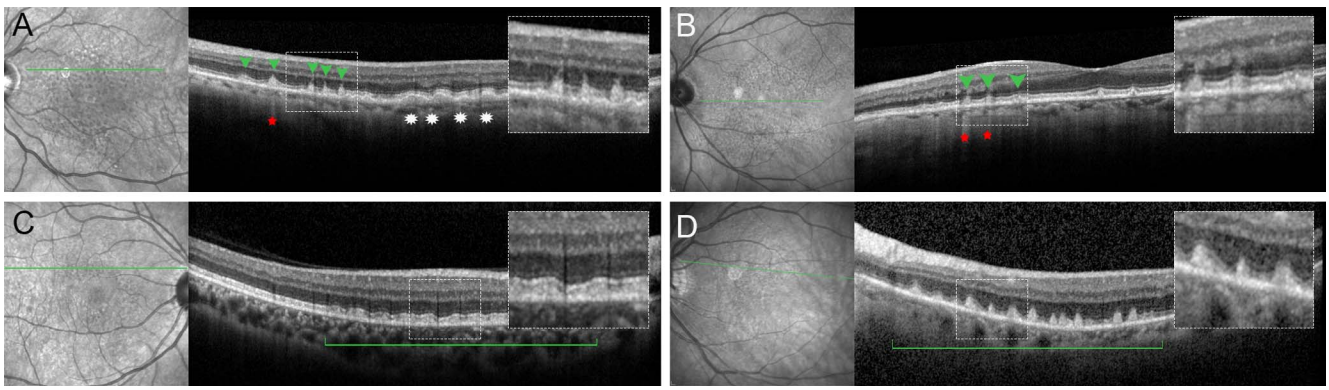

Figure 3. Representative SD-OCT images of RPD. *Horizontal axes* of the SD-OCT scans are indicated by *green lines* in the IR-R images. RPD present with hyperreflective interiors (*green arrowheads*; [**A**, **B**]) as opposed to the moderate reflectivity of classical drusen (*white asterisks*; [**A**]). Transmission into the choroid is a feature of some RPD (*red asterisks* in [**A**, **B**]) but not all (*green arrowheads* without *red asterisk* in [**A**]). Patient 7 (**A**), Patient 3 (**B**). RPD can present as intermittent thickening of the IZ and EZ bands (*green bracket* in [**C**]); Patient 1 (**C**). RPD also can present as sharp pyramidal lesions breaking through IZ and EZ bands (*green bracket* in [**D**]); Patient 23.

Investigative Ophthalmology & Visual Science

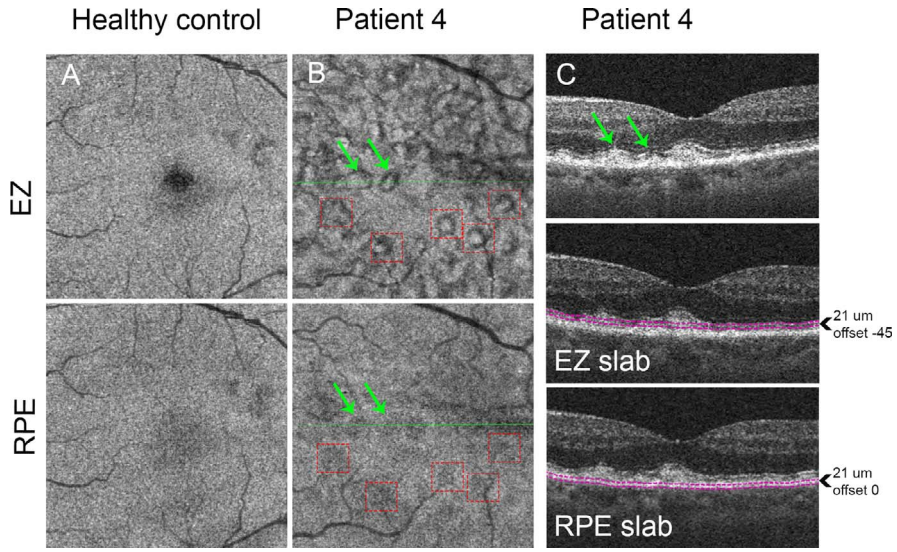

Figure 4. En face OCT images generated using the HD-OCT Zeiss Cirrus 5000. (**A**) En face OCT images (C-scan, 3 mm × 3 mm) in healthy eye (**A**) and RPD (Patient 4; **B**) at the level of the EZ and RPE. Angiography cube. En face images show changes in reflectivity corresponding to RPD lesions. (**B**) EZ slab demonstrates round lesions with darker edges and brighter hyperreflective center (examples are indicated by *red dotted rectangles*). RPE slab shows darker areas of reduced reflectivity at corresponding positions (*red dotted rectangles*). (**C**) OCT B-scan, corresponding to the en face images (**B**). Horizontal axis of B-scan is shown as *green lines* in EZ and RPE images (**B**). In the B-scan are two adjacent RPD lesions (*green arrows*) which also can be observed in the en face EZ and RPE slabs (*green arrows*; [**B**]). The *purple dotted lines* in the OCT B-scans (**C**) indicate the segmentation lines used to define EZ (*upper*) and RPE (*lower*) slabs in (**B**).

length of the scan due to axial tilt, media obstruction, or excessive vessel shadowing were excluded from analysis. Reflectivities recorded along the axes of the horizontal scans (Fig. 5, white traces) revealed downward deflections (reduced reflectivity) corresponding to RPD visible in the SD-OCT images. Reductions in reflectivity were less pronounced when RPE presented as shallow undulations and were broader at their base and more pronounced when the RPD were conically-shaped (e.g., P3). A second set of reflectivity profiles generated at right angles (coronal plane; Fig. 5, insets, and blue and red traces) showed that reductions in RPE/Bruch's membrane reflectivities were greater in association with RPD (Fig. 5, inset, red traces, and red vertical dotted lines) as compared to immediately adjacent regions (blue traces and blue dotted vertical lines). En face OCT images (Fig. 5, right panels) illustrated the colocalization of reflectivity reductions in RPE/Bruch's membrane and the EZ layer.

As can be seen in Figure 6, in all eyes exhibiting RPD lesions in SW-AF images, similar lesions were visible in NIR-AF and IR-R images and corresponding reflectivity changes were detected at the selected depths of the EZ and RPE in en face OCT images. In all patients, moreover, RPD visible in the fundus corresponded to alterations in horizontal SD-OCT scans that presented as corrugations of the IZ and EZ bands or prominent hyperreflective conical-shaped aberrations in photoreceptor-attributable SD-OCT bands (Figs. 2, 3).

Discussion

The NIR-AF signal emanates primarily from RPE melanin although there also is a minor contribution from choroidal melanocytes.[29,41–43] SW-AF, on the other hand, is emitted by the fluorescent bisretinoids of RPE lipofuscin that originate in photoreceptor cells and accumulate in RPE after phagocytic transfer.[44] We found that NIR-AF imaging enabled detection of RPD in central areas of the macula where macular pigment obscures visibility in SW-AF images. NIR-AF imaging for the detection of RPD was, in some cases, superior to SW-AF and IR-R because of the increased contrast afforded by NIR-AF.[45] A limitation of our study was that, although the SW-AF and SD-OCT findings were consistent with earlier work, not all patients were tested at the same time interval after disease onset and the patients were not followed longitudinally.

We observed that in NIR-AF and SW-AF images, RPD are relatively hypoautofluorescent, the darkened foci in SW-AF images colocalizing with similarly darkened foci in NIR-AF images (Figs. 1, 2). The reduced NIR-AF at positions of RPD is unlikely to be due to absorption by tissue anterior to the RPD, since the latter is negligible at wavelengths of 600 to 1300 nm.[46] We also have given consideration to the hyperreflectivity of the RPD lesion (as visualized in the photoreceptor-attributable SD-OCT bands) and whether the scattering could reduce NIR light transmission, and thereby account for the reduction of NIR-AF and IR-R (Figs.1, 2) originating in the RPE monolayer. However, the light that is reflected by the RPD is only a minor portion of NIR light that is delivered for OCT imaging. Moreover, reduced transmission into the choroid (viewed as a darkened column extending posterior to RPE/Bruch's membrane) is not observed in association with RPD and in some cases transmission is increased (Fig. 3). Additionally, if the darkened RPD foci in NIR-AF and IR-R fundus images were caused by scattering and reduced transmission through the lesion visible in photoreceptor cell attributable SD-OCT bands, one might expect the extent of darkening to vary with the stage of the RPD lesion (for instance, shallow corrugations versus conical lesions) in SD-OCT scans, but this is not observed. Fundus flecks in recessive Stargardt disease also present as hyperreflective lesions in photoreceptor-attributable OCT layers, and have an appearance that is strikingly similar to RPD.[47] Yet, the hyperreflectivity visible by SD-OCT imaging does not appear to determine lesion presentation in NIR-AF images. Specifically, flecks correspond to foci of absent NIR-AF in fundus images[47] while RPD in SD-OCT scans colocalize with NIR-AF that is reduced but not absent. For these reasons, we expect that the autofluorescence and reflectivity originating in RPE posterior

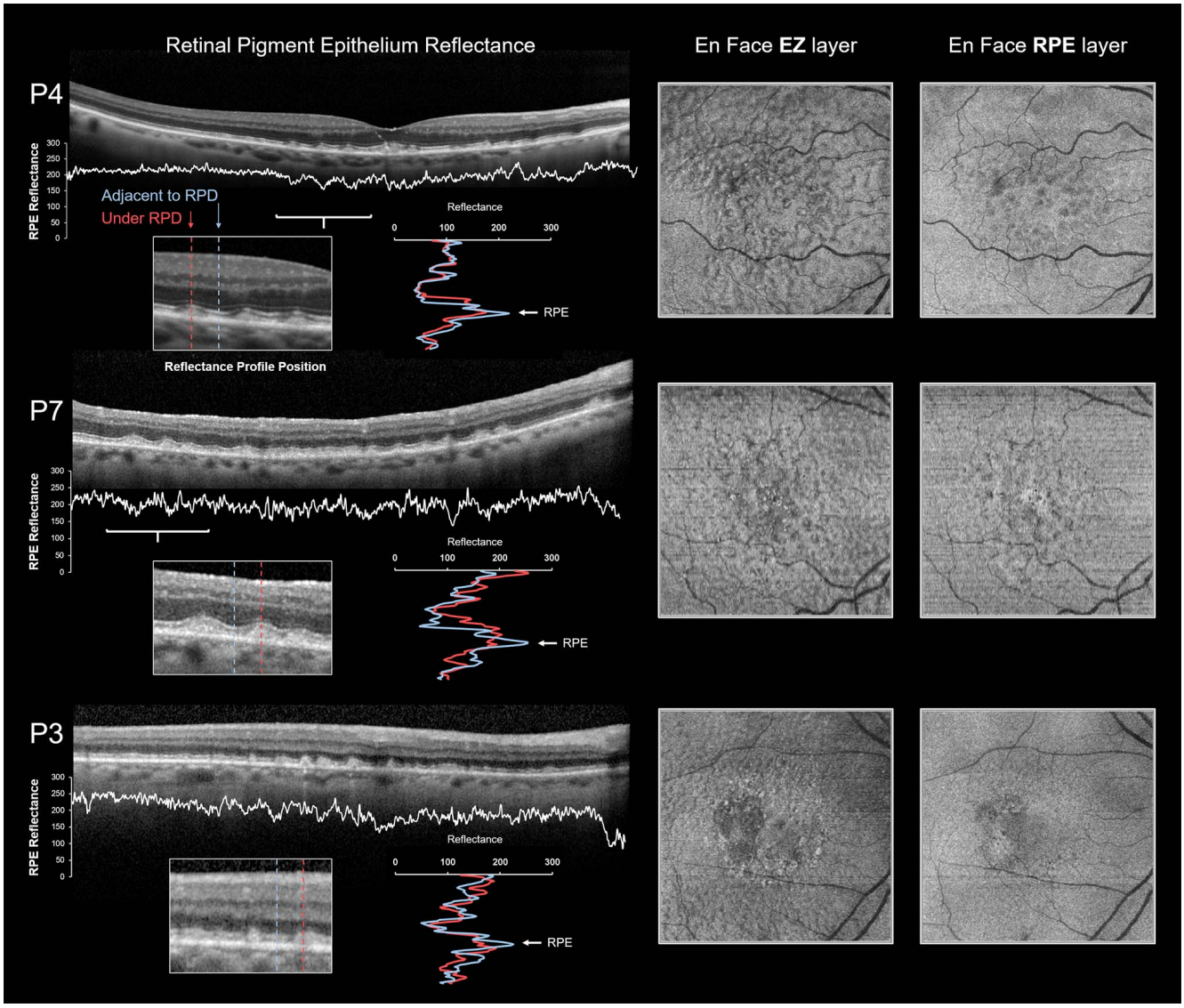

Figure 5. Reflectivity profiles generated from outer layers of retina. *Left*: RPE /Bruch's membrane reflectivity profile (*white trace*) extracted from OCT B-scans (Spectralis HRA+OCT). P4, P7, and P3. Below each SD-OCT B-scan the RPE-Bruch's membrane reflectivity profile is plotted as a *white trace. Insets* present magnified views of areas of SD-OCT scan indicated by a *white bracket* below the full scan. The corresponding coronal reflectivity profiles (*horizontal red* and *blue traces*) at positions on the expanded OCT scan are shown for reflectivities under the apical tip of RPD (*red trace*, *red vertical dashed line*) and adjacent to the RPD (*blue trace* and *blue vertical dashed line*). RPE reflectivity associated with RPD is reduced. *Right*: en face OCT images (HD-OCT Cirrus 5000) at levels of EZ and RPE in the same patients. Changes in reflectivity correspond to RPD lesions.

to the RPD, are a sign of changes in the RPE and are not imposed by the hyperreflectivity of the RPD.

RPD detected in the fundus by NIR-AF, SW-AF, and IR-R imaging corresponded, in horizontal SD-OCT scans, to changes in the contour and reflectivity of EZ in some cases and to conical hyperreflective lesions anterior to the RPE/Bruch's membrane band in other cases. These lesions also could extend radially through the EZ photoreceptor-attributable SD-OCT band and become associated with visible ONL thinning. It has been pointed out that the periodicity of the triangular-shaped reflectivity deposits prominently visible in horizontal SD-OCT scans (Figs. 2, 3) cannot explain the RPD patterning observed in fundus images.[27] On the other hand, these lesions together with early-stage RPD presenting as undulations of outer retina[2,37] (Figs. 2, 3) do have sufficient regularity to account for the RPD network.

In NIR reflectance fundus images, RPD present as darkened lesions. With C-scan reconstruction of the OCT images, and alignment to the plane of the EZ and RPE, hyperreflective ovoid or round areas at the level of the EZ in en face SD-OCT were aligned spatially with hyporreflective ovoid or round foci viewed in the RPE band. As discussed above, the lesions in en face images of RPE cannot be attributed to optical shadowing (interception of light by an opaque substance) since light in the NIR range (700–1400 nm) is absorbed only weakly by biological tissues. cSLO images produced using 870 nm light are primarily determined by reflected light.[48] RPE melanin is a reflector[36,49,50] and major contributor to the intensity of the RPE/Bruch's band in SD-OCT.[51] Thus, it is reasonable to suggest that the reduced reflectivity in the en face OCT images positioned within the boundaries of the RPE is due to a reduction in RPE melanin reflectivity. This interpretation is consistent with the reduced melanin associated–NIR-AF signal

Investigative Ophthalmology & Visual Science

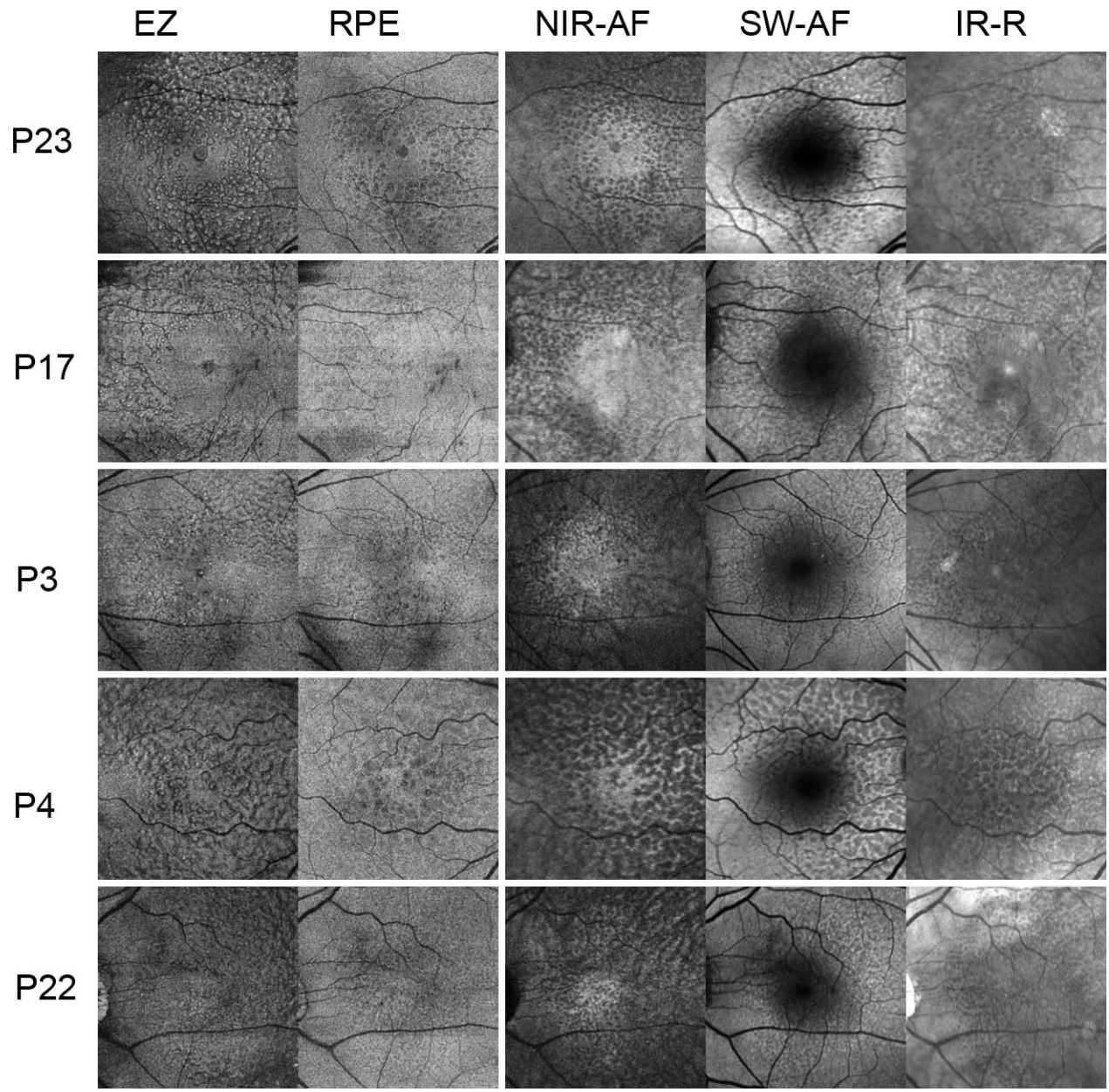

Figure 6. Compilation of fundus images illustrating patterns of reticular pseudodrusen visible with en face OCT at the level of EZ and RPE (Zeiss Cirrus 5000). Also shown are NIR-AF, SW-AF, and IR-R images obtained with the Heidelberg Spectralis and Heidelberg HRA2 (Heidelberg Engineering). P, patient. All patients presented with a phenotype consisting of predominantly pseudodrusen.

associated with RPD in fundus images. The presence of increased transmission of optical signals posterior to the RPE, in the case of some RPD[24] (Fig. 3) is indicative of more advanced RPE disease.

We suggest that the RPD lesions observed in the photoreceptor-attributable layers of SD-OCT scans denote photoreceptor cells that are undergoing a degenerative process that begins in outer segments and progresses radially. These photoreceptor cells may be degenerating secondary to RPE changes. Imaging by SW-AF and NIR-AF, together with en face OCT, indicates that the configurations recognized as RPD are associated with periodic abnormalities in the RPE monolayer. Perhaps the reticular patterning can be accounted for by cellular reorganization undertaken to fill gaps in the RPE monolayer left by cell loss. Under such a process, RPE cell drop-out would be the nidus of RPD organization. Remodeling of the RPE layer, through processes of cell migration and spreading and concomitant thinning, could account for the reduced signal originating in RPE: reduced melanin signal detected as NIR-AF; reduced reflectivity observed in en face OCT images and diminished SW-AF. This premise is consistent with the irregularities in the shape and size of RPE observed in association with RPD in histologic material.[24] Perhaps when the ability of the RPE cells to compensate for the loss of neighbors is exhausted, atrophic areas form. Herein would be an explanation for the association between RPD disease and GA. Considerable remodeling of the RPE monolayer has been reported in normal aging with an increase in large RPE cells being indicative of compensation for cell loss.[52] RPE changes with the possibility of accompanying cell dysfunction and a

Investigative Ophthalmology & Visual Science

loss of trophic support for the choriocapillaris also could explain the reduced choroidal thickness that has been reported in association with RPD.[53–55]

Acknowledgments

Supported by grants from the National Eye Institute (NEI, Bethesda, MD; EY024091 and P30EY019007); The New York Community Trust; and a grant from Research to Prevent Blindness to the Department of Ophthalmology, Columbia University.

Disclosure: **M. Paavo**, None; **W. Lee**, None; **J. Merriam**, None; **S. Bearelly**, None; **S. Tsang**, None; **S. Chang**, None; **J.R. Sparrow**, None;

References

1. Mimoun G, Soubrane G, Coscas G. Macular drusen. *J Fr Ophtalmol*. 1990;13:511–530.
2. Zweifel SA, Spaide RF, Curcio CA, Malek G, Imamura Y. Reticular pseudodrusen are subretinal drusenoid deposits. *Ophthalmology*. 2010;117:303–312.e1.
3. Wu Z, Ayton LN, Luu CD, Baird PN, Guymer RH. Reticular pseudodrusen in intermediate age-related macular degeneration: prevalence, detection, clinical, environmental, and genetic associations. *Invest Ophthalmol Vis Sci*. 2016;57:1310–1316.
4. Chan H, Cougnard-Gregoire A, Delyfer MN, et al. Multimodal imaging of reticular pseudodrusen in a population-based setting: the Alienor Study. *Invest Ophthalmol Vis Sci*. 2016;57:3058–3065.
5. Lee MY, Yoon J, Ham DI. Clinical features of reticular pseudodrusen according to the fundus distribution. *Br J Ophthalmol*. 2012;96:1222–1226.
6. Sivaprasad S, Bird A, Nitiahpapand R, et al. Perspectives on reticular pseudodrusen in age-related macular degeneration. *Surv Ophthalmol*. 2016;61:521–537.
7. Suzuki M, Sato T, Spaide RF. Pseudodrusen subtypes as delineated by multimodal imaging of the fundus. *Am J Ophthalmol*. 2014;157:1005–1012.
8. Alten F, Eter N. Current knowledge on reticular pseudodrusen in age-related macular degeneration. *Br J Ophthalmol*. 2015;99:717–722.
9. Smith RT, Sohrab MA, Busuioc M, Barile G. Reticular macular disease. *Am J Ophthalmol*. 2009;148:733–743.
10. Zweifel SA, Imamura Y, Spaide TC, Fujiwara T, Spaide RF. Prevalence and significance of subretinal drusenoid deposits (reticular pseudodrusen) in age-related macular degeneration. *Ophthalmology*. 2010;117:1775–1781.
11. Curcio CA, Messinger JD, Sloan KR, McGwin G, Medeiros NE, Spaide RF. Subretinal drusenoid deposits in non-neovascular age-related macular degeneration: morphology, prevalence, topography, and biogenesis model. *Retina*. 2013;33:265–276.
12. Delori FC, Goger DG, Dorey CK. Age-related accumulation and spatial distribution of lipofuscin in RPE of normal subjects. *Invest Ophthalmol Vis Sci*. 2001;42:1855–1866.
13. Greenberg JP, Duncker T, Woods RL, Smith RT, Sparrow JR, Delori FC. Quantitative fundus autofluorescence in healthy eyes. *Invest Ophthalmol Vis Sci*. 2013;54:5684–5693.
14. Flamendorf J, Agron E, Wong WT, et al. Impairments in dark adaptation are associated with age-related macular degeneration severity and reticular pseudodrusen. *Ophthalmology*. 2015;122:2053–2062.
15. Steinberg JS, Sassmannshausen M, Fleckenstein M, et al. Correlation of partial outer retinal thickness with scotopic and mesopic fundus-controlled perimetry in patients with reticular drusen. *Am J Ophthalmol*. 2016;168:52–61.
16. Wu Z, Ayton LN, Makeyeva G, Guymer RH, Luu CD. Impact of reticular pseudodrusen on microperimetry and multifocal electroretinography in intermediate age-related macular degeneration. *Invest Ophthalmol Vis Sci*. 2015;56:2100–2106.
17. Lee MY, Yoon J, Ham DI. Clinical characteristics of reticular pseudodrusen in Korean patients. *Am J Ophthalmol*. 2012;153:530–535.
18. van Grinsven MJJP, Buitendijk GHS, Brussee C, et al. Automatic identification of reticular pseudodrusen using multimodal retinal image analysis. *Invest Ophthalmol Vis Sci*. 2015;56:633–639.
19. Finger RP, Chong E, McGuinness MB, et al. Reticular pseudodrusen and their association with age-related macular degeneration: The Melbourne Collaborative Cohort Study. *Ophthalmology*. 2016;123:599–608.
20. Marsiglia M, Boddu S, Bearelly S, et al. Association between geographic atrophy progression and reticular pseudodrusen in eyes with dry age-related macular degeneration. *Invest Ophthalmol Vis Sci*. 2013;54:7362–7369.
21. Grewal DS, Chou J, Rollins SD, Fawzi AA. A pilot quantitative study of topographic correlation between reticular pseudodrusen and the choroidal vasculature using en face optical coherence tomography. *PLoS One*. 2014;9:e92841.
22. Sohrab MA, Smith RT, Salehi-Had H, Sadda SR, Fawzi AA. Image registration and multimodal imaging of reticular pseudodrusen. *Invest Ophthalmol Vis Sci*. 2011;52:5743–5748.
23. Spaide RF. Colocalization of pseudodrusen and subretinal drusenoid deposits using high-density en face spectral domain optical coherence tomography. *Retina*. 2014;34:2336–2345.
24. Greferath U, Guymer RH, Vessey KA, Brassington K, Fletcher EL. Correlation of histologic features with in vivo imaging of reticular pseudodrusen. *Ophthalmology*. 2016;123:1320–1331.
25. Khan KN, Mahroo OA, Khan RS, et al. Differentiating drusen: drusen and drusen-like appearances associated with ageing, age-related macular degeneration, inherited eye disease and other pathological processes. *Prog Retin Eye Res*. 2016;53:70–106.
26. Meadway A, Wang X, Curcio CA, Zhang Y. Microstructure of subretinal drusenoid deposits revealed by adaptive optics imaging. *Biomed Opt Express*. 2014;5:713–727.
27. Heiferman MJ, Fernandes JK, Munk M, Mirza RG, Jampol LM, Fawzi AA. Reticular pseudodrusen on infrared imaging are topographically distinct from subretinal drusenoid deposits on en face optical coherence tomography. *Retina*. 2015;35:2593–2603.
28. Ueda-Arakawa N, Ooto S, Nakata I, et al. Prevalence and genomic association of reticular pseudodrusen in age-related macular degeneration. *Am J Ophthalmol*. 2013;155:260–269 e262.
29. Keilhauer CN, Delori FC. Near-infrared autofluorescence imaging of the fundus: visualization of ocular melanin. *Invest Ophthalmol Vis Sci*. 2006;47:3556–3564.
30. Ferris FL III, Wilkinson CP, Bird A, et al. Clinical classification of age-related macular degeneration. *Ophthalmology*. 2013;120:844–851.
31. Staurenghi G, Sadda S, Chakravarthy U, Spaide RF. Proposed lexicon for atomic landmarks in normal posterior segment spectral-domain optical coherence tomography: The IN*OCT consensus. *Ophthalmology*. 2014;121:1572–1578.
32. Schindelin J, Arganda-Carreras I, Frise E, et al. Fiji: an open-source platform for biological-image analysis. *Nat Methods*. 2012;9:676–682.
33. Nesper PL, Soetikno BT, Fawzi AA. Choriocapillaris Nonperfusion is Associated With Poor Visual Acuity in Eyes With Reticular Pseudodrusen. *Am J Ophthalmol*. 2017;174:42–55.

34. De Bats F, Mathis T, Mauget-Faysse M, Joubert F, Denis P, Kodjikian L. Prevalence of reticular pseudodrusen in age-related macular degeneration using multimodal imaging. *Retina*. 2016;36:46–52.
35. Nolan JM, Stringham JM, Beatty S, Snodderly DM. Spatial profile of macular pigment and its relationship to foveal architecture. *Invest Ophthalmol Vis Sci*. 2008;49:2134–2142.
36. Ly A, Nivison-Smith L, Assaad N, Kalloniatis M. Infrared reflectance imaging in age-related macular degeneration. *Ophthalmic Physiol Opt*. 2016;36:303–316.
37. Querques G, Canoui-Poitrine F, Coscas F, et al. Analysis of progression of reticular pseudodrusen by spectral domain-optical coherence tomography. *Invest Ophthalmol Vis Sci*. 2012;53:1264–1270.
38. Querques G, Srour M, Massamba N, Puche N, Souied EH. Reticular pseudodrusen. *Ophthalmology*. 2013;120:872.e4.
39. Querques G, Querques L, Martinelli D, et al. Pathologic insights from integrated imaging of reticular pseudodrusen in age-related macular degeneration. *Retina*. 2011;31:518–526.
40. Steinberg JS, Gobel AP, Fleckenstein M, Holz FG, Schmitz-Valckenberg S. Reticular drusen in eyes with high-risk characteristics for progression to late-stage age-related macular degeneration. *Br J Ophthalmol*. 2015;99:1289–1294.
41. Delori FC, Keilhauer C, Sparrow JR, Staurenghi G. Origin of fundus autofluorescence. In: Holz FG, Schmitz-Valckenberg S, Spaide RF, Bird AC, eds. *Atlas of Fundus Autofluorescence Imaging*. Berlin Heidelberg: Springer-Verlag; 2007:17–29.
42. Schmitz-Valckenberg S, Lara D, Nizari S, et al. Localisation and significance of in vivo near-infrared autofluorescent signal in retinal imaging. *Br J Ophthalmol*. 2011;95:1134–1139.
43. Gibbs D, Cideciyan AV, Jacobson SG, Williams DS. Retinal pigment epithelium defects in humans and mice with mutations in MYO7A: imaging melanosome-specific autofluorescence. *Invest Ophthalmol Vis Sci*. 2009;50:4386–4393.
44. Sparrow JR, Gregory-Roberts E, Yamamoto K, et al. The bisretinoids of retinal pigment epithelium. *Prog Retin Eye Res*. 2012;31:121–135.
45. Duncker T, Marsiglia M, Lee W, et al. Correlations amongst near-infrared and short-wavelength autofluorescence and spectral domain optical coherence tomography in recessive Stargardt disease. *Invest Ophthalmol Vis Sci*. 2014;55:8134–8143.
46. Tsai CL, Chen JC, Wang WJ. Near-infrared absorption property of biological soft tissue constituents. *J Med Biol Eng*. 2001;21:7–14.
47. Sparrow JR, Marsiglia M, Allikmets R, et al. Flecks in recessive Stargardt disease: short-wavelength autofluorescence, near-infrared autofluorescence, and optical coherence tomography. *Invest Ophthalmol Vis Sci*. 2015;56:5029–5039.
48. Elsner AE, Burns SA, Weiter JJ, Delori FC. Infrared imaging of sub-retinal structures in the human ocular fundus. *Vision Res*. 1996;36:191–205.
49. Theelen T, Berendschot TT, Hoyng CB, Boon CJ, Klevering BJ. Near-infrared reflectance imaging of neovascular age-related macular degeneration. *Graefes Arch Clin Exp Ophthalmol*. 2009;247:1625–1633.
50. Zhang QX, Lu RW, Messinger JD, Curcio CA, Guarcello V, Yao XC. In vivo optical coherence tomography of light-driven melanosome translocation in retinal pigment epithelium. *Sci Reports*. 2013;3:2644.
51. Wilk MA, Huckenpahler AL, Collery RF, Link BA, Carroll J. The effect of retinal melanin on optical coherence tomography images. *Trans Vis Sci Tech*. 2017;6(2):8.
52. Ach T, Huisingh C, McGwin G Jr, et al. Quantitative autofluorescence and cell density maps of the human retinal pigment epithelium. *Invest Ophthalmol Vis Sci*. 2014;55:4832–4841.
53. Spaide RF. Outer retinal atrophy after regression of subretinal drusenoid deposits as a newly recognized form of late age-related macular degeneration. *Retina*. 2013;33:1800–1808.
54. Querques G, Querques L, Forte R, Massamba N, Coscas F, Souied EH. Choroidal changes associated with reticular pseudodrusen. *Invest Ophthalmol Vis Sci*. 2012;53:1258–1263.
55. Garg A, Oll M, Yzer S, et al. Reticular pseudodrusen in early age-related macular degeneration are associated with choroidal thinning. *Invest Ophthalmol Vis Sci*. 2013;54:7075–7081.

Investigative Ophthalmology & Visual Science